# Design and Development of *Gamera*: A Human Powered Helicopter from the University of Maryland

Joseph Schmaus, Benjamin Berry, Graham Bowen-Davies, Brandon Bush, Chen Friedman, Mor Gilad, Ananth Sridharan, William Staruk, Benjamin Woods
Graduate Students

Alfred Gessow Rotorcraft Center
Department of Aerospace Engineering
University of Maryland, College Park, MD 20742

## ABSTRACT

***Gamera*, a human powered helicopter designed and constructed by students at the University of Maryland flew several times in 2011 with a maximum recorded flight time of 11.4 seconds. Aerodynamic modeling agreed with full scale testing that was performed and showed that the vehicle was capable of hovering with 0.8 horsepower. To achieve this low power vehicle, structurally efficient design techniques were applied to the rotor, airframe and transmission. Pilots were trained to output the required power for the longest possible flight duration. *Gamera* is a first significant step in the quest for the Sikorsky Prize.**

## INTRODUCTION

The AHS Igor I. Sikorsky Human Powered Helicopter (HPH) prize was developed to promote development of the dream of human powered hovering fight. Initially offered in 1980, it is to be awarded to the first team to fly a helicopter, under human power only, for at least 60 seconds and reach 3 m (9.8 ft) above the ground at some point during the flight. To ensure hovering flight, drift is limited to a box of 10 m (32.8 ft) square around the point of liftoff.

Historically inspired by Leonardo da Vinci's conceptual illustration of an "air screw", and bolstered by the recent successes of human powered airplanes, the pursuit of sustained human-powered vertical flight has received renewed attention in the last few decades. Recent advances in lightweight construction materials and manufacturing techniques have placed requirements of human powered vertical flight at the boundaries of attainable peak human performance and rotorcraft design optimization. Two primary challenges need to be overcome to realize human powered vertical flight. First, aerostructural optimizations are required to minimize hover power. Second, sustained power outputs approaching 1 hp for up to 60 seconds from human pilots requires specialized high-performance training and diets. Still, even with these optimizations, theoretical predictions on whether human-powered vertical flight is possible can be contradictory or inconclusive [1, 2].

No vehicle has yet completed the requirements set by the Sikorsky prize, and in the 31 years of the competition, only 3 vehicles have successfully hovered at all. These include 8 seconds from the Cal Poly *Da Vinci III* and 19.5 second Nihon University *Yuri-I*. The most recent to achieve this milestone on the way to the Sikorsky Prize, with an official Fédération Aéronautique Internationale (FAI) world record for a hover duration of 11.4 seconds (general and feminine categories), is Team *Gamera* of the Alfred Gessow Rotorcraft Center at the University of Maryland.

*Gamera* Human Powered Helicopter team was formed in 2008 by a group of University of Maryland engineering faculty and students. As of 2011, the team has had more than 70 members: undergraduate, graduate and faculty from a variety of disciplines. Building upon the research and design experience at the Alfred Gessow Rotorcraft Center, Team *Gamera* has taken on the challenge of performing the analysis, testing, construction, athletic training and flight of the *Gamera* HPH. Limited published data is available for *Gamera*'s flight regime and human power requirements, therefore extensive testing in a variety of areas was performed prior to construction. This paper presents the aerodynamic and structural aspects of the rotor, airframe, transmission and the human powerplant and how they were developed for the July18th, 2011 flight of *Gamera*.

## ROTOR AERODYNAMIC DESIGN

*Gamera*, shown in Figure 1 and with critical dimensions listed in the appendix, is a quadrotor helicopter with an airframe consisting of interconnecting trusses and a cockpit. There are many strongly interacting design variables to consider for HPH. One of the most important among these is choice of pilot.

For HPH, the weight of the pilot and the power she is capable of automatically show strong differences from traditional helicopters. For a typical lightweight helicopter (e.g. Robinson *R22*) the power loading is about 10 lb/hp (6.1 kg/kW), while for *Gamera* this value turns out to be closer to 270 lb/hp (160 kg/kW). The disc loading is another good example: conventional values are on the order of 2.7 lb/ft$^2$

Presented at the American Helicopter Society Future Vertical Lift Aircraft Design Conference, January 18-20, 2012, San Francisco, California. 

(64 kg/m$^2$) for the Robinson *R22*, while for *Gamera* it is on the order of 0.05 lb/ft$^2$ (1.2 kg/m$^2$). This places the design of the human powered helicopter in an uncharted territory where well established helicopter design rules may not be applicable.

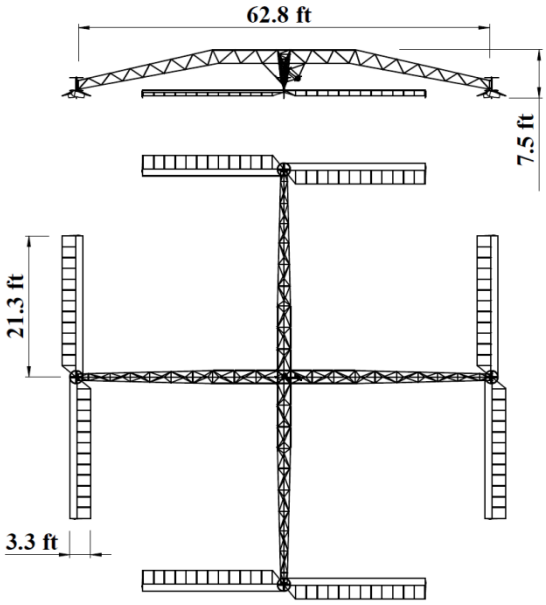


**Figure 1. 2-view of *Gamera* HPH**

**Aerodynamics of Rotors in Ground Effect**

In hovering flight, power is expended for two tasks: the first, to sustain the total vehicle lift (induced power), and the second, to overcome profile drag while spinning the blades (profile power). The induced power depends on the rotor disk loading, while the profile power depends on blade plan-form area, airfoil section and rotor RPM.

All human powered flying vehicles (fixed wing and helicopters) depend on ground effect to reduce induced power. As aircraft approach the ground they see a decrease in the induced power required for a given weight. This phenomenon occurs because of constructive interference between the ground plane and the induced velocity of the lifting surface. Traditionally, ground effect for rotors is applied as a percentage change in the power required as a function of non-dimensional height z/R, where z is rotor hub height an R is the rotor radius. This value often has a lower practical limit of 0.5 because of rotor placement above the helicopter fuselage. In HPH rotors, the hub is placed as close to the ground as possible to maximize ground effect. Combined with large radii rotors, z/R can be as low as 0.1, leading to total power savings of up to 70% [3].

Previous experience and momentum theory results indicate that operating at reduced rotor speeds (10-20 RPM) is critical to minimizing profile power. This results in a tip Reynolds number between 500,000 and 900,000. Sections further inboard are expected to experience boundary layer transition (from laminar to turbulent), and airfoil sensitivity to Reynolds number must be considered. Among the many airfoils designed for low Reynolds number flight, the Eppler387 airfoil was selected for these blades. In addition to favorable aerodynamic characteristics [4], this airfoil has a concave lower surface that is shallower than many comparable airfoils, greatly simplifying manufacturing.

The methodology used for a majority of the present analysis is based on the classical blade element momentum theory (BEMT) [2]. Additionally, a Finite Element Method (FEM) based structural model was coupled with the BEMT to incorporate elastic flap-wise bending and torsion into the solution. Ground effect was modeled as a reduction of induced inflow, which depends on the height above the ground of the lifting surface. Low weight blades permit large blade deflections which motivated that this inflow reduction be implemented on an elemental level and coupled to the FEM deflections, rather than as a global effect. 2-D airfoil wind-tunnel data tables were used for lift, drag, and pitching moment characteristics. More details and a rigorous validation of this method can be found in Gilad [3].

**Vehicle Configuration**

The first fundamental design decision made was that a quadrotor with 2 bladed rotors would be the most promising configuration to attempt. This was made using simple momentum theory calculations [2]. The main reason for selecting this configuration lies in its inherent stability as demonstrated by Yuri I [5]. Other attempts utilized either tip driven single rotors or coaxial rotors, which faced challenges due to weight and stability issues. A comprehensive analysis of human powered helicopters with some detailed review of past experience can be found in the work by Hawkins [6].

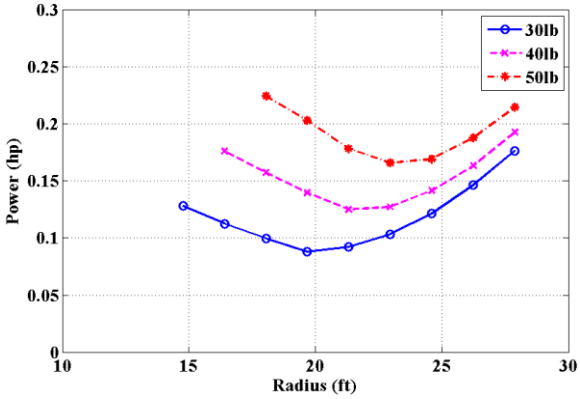


**Figure 2. Single rotor performance at various weights and radii (BEMT predictions)**

The induced power (and to a lesser extent, the profile power) is a strong function of gross take-off weight. A first order model for empty weight of the vehicle, combined with a pilot power-weight curve, is critical for obtaining accurate performance predictions. Using the *Yuri-I* as a starting point, a series of trade studies converged on the final design (presented for a single rotor). From an aerodynamic perspective, increased radius reduces induced power while

increasing profile power. Parametric studies of the impact of rotor radius on power required at constant thrust are shown in Figure 2. With increasing thrust, the optimal radius increases, and the vehicle dimensions grow proportionally. However, an upper limit for this parameter was set at 21.3 ft (6.5 m) to allow the vehicle to fit inside candidate test locations.

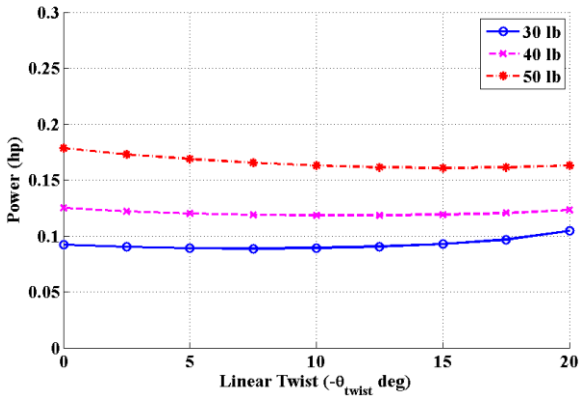


**Figure 3. Single rotor performance at various weights and linear twist rates (BEMT predictions)**

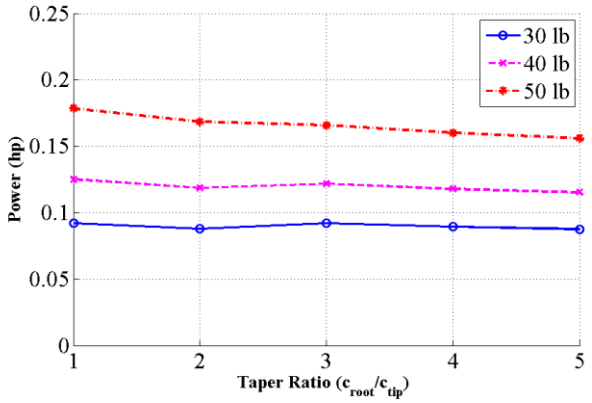


**Figure 4. Single rotor performance at various weights and linear taper rates (BEMT predictions)**

Helicopter theory instructs that the optimal hovering rotor has hyperbolically twisted and tapered rotor blades to minimize total power. Linear twist and taper, which is easier to implement on rotor blades, have shown significant power savings in many helicopters [2]. Twist and taper shown in Figure 3 and Figure 4 show noticeable improvements in power. However, blade twist and taper limit the utility of interchangeable parts, complicate construction techniques and increase build time. With these practical constraints in mind, penalties associated with not implementing twist and taper were accepted.

Rotor speed was initially set at 15 RPM. Rigorous analyses and experiments showed that the speed had to be increased to 19 RPM to avoid stall along the blade and the associated drag penalties. Figure 5 illustrates the impact of weight and RPM on the power required.

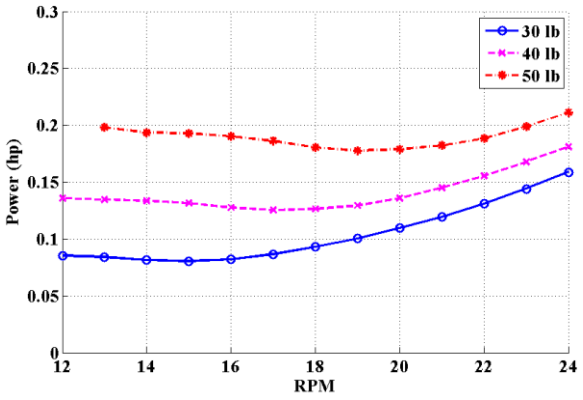


**Figure 5. Single rotor performance at various weights and rotor speeds (BEMT predictions)**

The design target was set at building a vehicle with an empty weight of 100 lb (45 kg) and a gross takeoff weight of 200 lb (90 kg). Analysis predicted that the power required to sustain hover at 2 ft (0.6 m) above the ground would be 0.7 hp (533 W).

### Aerodynamic Performance Testing

The analytical prediction was compared to experimental results to justify the design approach. Two in-house experiments designated for study of extreme ground effect were used for further validation in extreme ground effect ($z/R < 0.3$). These setups include the sub-scale Ground Effect Test Rig (GETR) and the full-scale Blade Balancing Rig (BBR). Results from these experiments were used in carrying out the validations of the methods proposed in this work. The full-scale experimental stand was also used to test several design modifications that proved challenging to model.

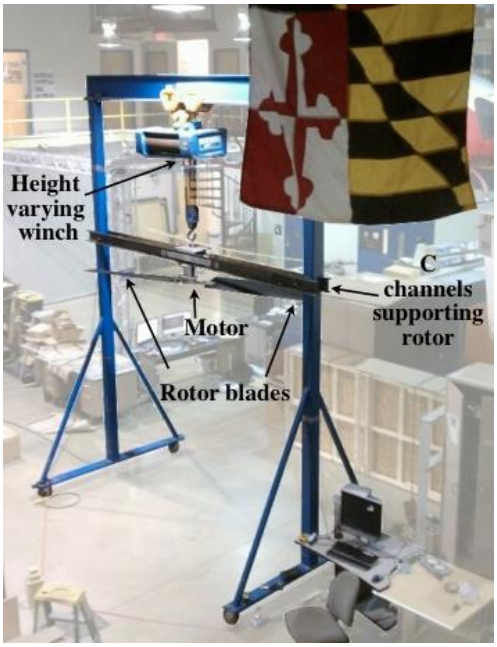


**Figure 6. Sub-scale Ground Effect Test Rig (GETR)**

GETR, shown in Figure 6, has variable-height capability, from 0-10.8 ft (0-3.3 m), which corresponded to z/R from 0 to 2.4. The test stand was powered by a 0.125 hp (93 W) electric motor and was instrumented with thrust, torque, and RPM sensors. The rotor studied was sub-scale and consists of two effectively rigid, untwisted, untapered, uniform NACA0012 blades, 4.5 ft (1.4 m) in radius and 0.89 ft (0.3 m) in chord. Blade pitch, RPM and height above ground were varied throughout testing. Thrust and torque were measured for each run using a coupled thrust-torque cell, and RPM is measured using a Hall sensor. The operational tip Reynolds number at 80 RPM was 200,000.

The power measured at various heights is non-dimensionalized by the power of the rotor when operating at a z/R of 2. At this height ratio, the rotor is considered to be effectively out of ground effect. $P_{IGE}$ and $P_{OGE}$ respectively define rotor power in ground effect and out of ground effect.

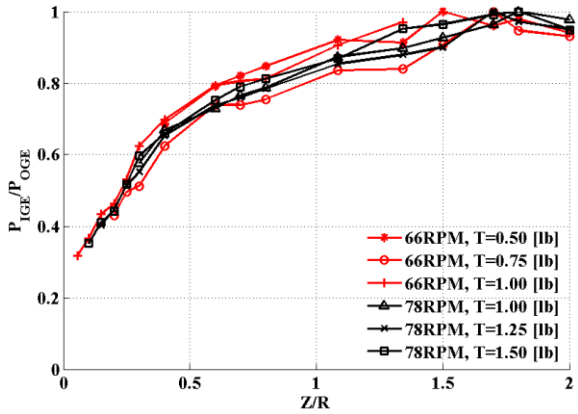


**Figure 7. Plot of GETR (sub-scale) performance at various RPM and thrust**

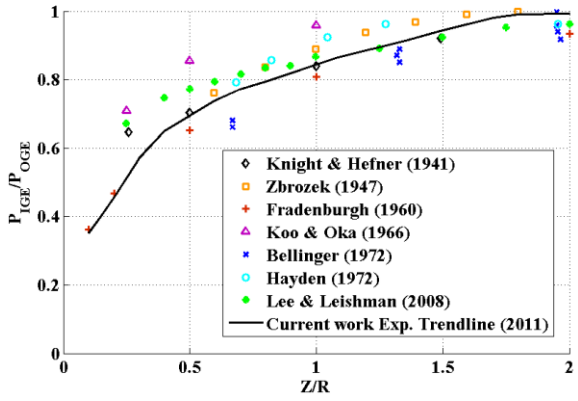


**Figure 8. Previous ground effect experiments compared to GETR (sub-scale) interpolated trend line [3]**

Resulting $P_{IGE}/P_{OGE}$ ratios for constant thrust are shown in Figure 7 for various height cases of the GETR test set up. Significant power reductions, consistent with previous experiments, are evident at low heights ($z/R < 0.4$) in this plot. An averaged trend-line based on the newly generated test data from the rigid sub-scaled rotor is then compared to past results, in Figure 8**,** and shows a good overall agreement. This new trend line, extracted from data in the z/R regime of interest, is used as the BEMT ground effect model described earlier.

BBR in Figure 9 was assembled to test full-scale rotor performance independent of the pilot, transmission, and structure. This tool was indispensable in measuring rotor power required, validating design codes, developing rotor subsystems and troubleshooting issues that are unique to *Gamera*. The BBR setup consisted of a 0.5 hp (373 W) DC motor connected to the rotor shaft using a chain system with an effective gear ratio of 78:1. The shaft was instrumented with strain gages for measuring torque and a Hall sensor for RPM. Four load cells are used to calculate the steady thrust and fixed-frame hub moments. The lightweight hub design used in *Gamera* necessitates a fixed pitch adjustment during each test and accurate moment data is critical for aerodynamically balancing the blades. All data is collected using LabVIEW and a National Instruments DAQ system at a rate of 1 kHz. For a rotor speed of 18 RPM, this provides more than 3000 samples per revolution.

**Figure 9. Full-scale Blade Balancing Rig (BBR)**

The test set-up was usually positioned with the rotor hub at 2 ft (0.6 m or $z/R_{hub}$ of 0.09) which corresponds to the design flight condition. Tests were also carried out at 4 ft (1.2 m or $z/R_{hub}$ of 0.18) to quantify possible performance variations that might result from excess available power. Thrust and torque were measured throughout for various settings of pitch and RPM.

Early models suggested 15 RPM as the design operational speed, but BBR data indicated that stall was reached before the target 50 lb (23 kg) of thrust. The test matrix was expanded to explore higher RPMs. Thrusts in excess of 50 lb (23 kg) were measured at 18 RPM, with a slight decrease in rotor power.

For validation of the BEMT formulation in extreme ground effect for a flexible rotor, calculated results were compared to full-scale experimental data from BBR at $z/R_{hub}$ = 0.09 and 18 RPM. This comparison, shown in Figure 10, includes BEMT predictions for performance of the rotor using both a rigid blade model and a flexible blade model.

Accounting for blade flexibility, especially the effect of ground vicinity substantially improves correlation with test data for all thrusts.

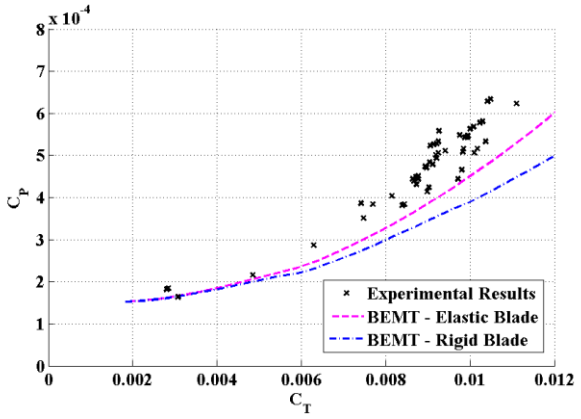


**Figure 10. Validation of BEMT method against BBR (full-scale) experiments at $z/R_{hub}$ = 0.09**

Low rotational speeds and light blades result in low centrifugal stiffening on an HPH; even with a fixed-pitch hub, significant bending displacements are seen in flap. The consequence of large-radii flexible blades is that small thrust differences can induce asymmetric flap bending and therefore asymmetric ground effect benefits (this is not a cyclic response as one blade has a consistently higher tip deflection throughout one revolution). Mechanical limitations in fine pitch control at the hub yielded several unbalanced pitch cases. Therefore most testing was performed with dimensional thrust varying with RPM rather than $C_T$ varying with pitch as would be ideal. This imbalance is reflected in the scatter of Figure 11 and the experiments used for validation in Figure 10 were selected from cases that were well balanced.

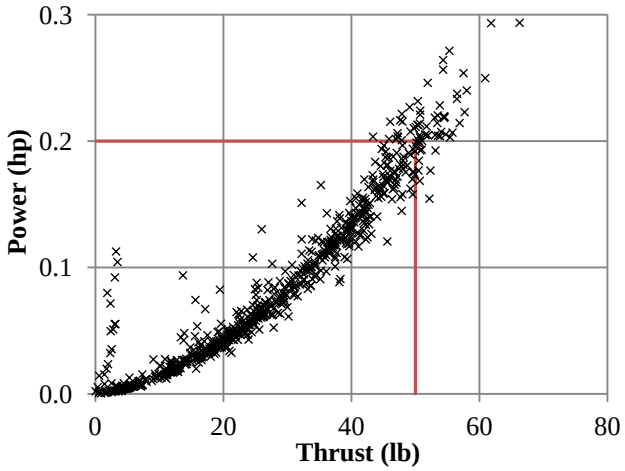


**Figure 11. BBR (full-scale) tests at $z/R_{hub}$ = 0.09**

The red lines in Figure 11 at 50 lb (23 kg) and 0.2 hp (150 W) show that design thrust and power were attainable at a $z/R_{hub}$ of 0.09. With all four rotors, this yields an experimental power required of 0.8 hp (597 W), disregarding transmission losses. Biasing the rotor tips towards the ground using negative precone helps reduce tip deflections in flight. The minimum-power cases in Figure 11 correspond to small negative precone angles and suggested that significant power savings could be realized with this simple adjustment. Ultimately this power savings was essential as the actual gross take-off weight shown in the appendix required an actual thrust of 54.5 lb (24.3 kg) from each rotor, placing 0.2 hp at the bottom side of the experimental envelope.

At high RPM, the thrust imbalance between the blades was observed to diverge, dramatically tilting the tip-path-plane. This phenomenon was poorly understood during early stages of testing and delayed system integration and rotor balancing. Systematic testing identified that this phenomenon is due to coupling between flap and torsion brought on by variations in the elastic stiffness of individual blades. Pairing blades that had identical performance and operating at lower RPMs helped mitigate the issue. BBR was essential in identifying identical pairs of blades and the critical RPM that minimizes rotor power while avoiding the divergence condition.

The BBR was used as a platform for evaluating the relative merit of various design modifications. Typically, these evaluations were performed as A to B comparisons at a fixed, balanced pitch at various RPMs. Depending on the nature of the modification, thrust and/or power were strongly affected, so power loading was used to evaluate effectiveness of the attempted modifications.

Centrifugal pumping of air through a hollow blade has inherent power penalties. In early helicopters, varying distribution of internal pressures caused deformation of the airfoil cross section in blades with rigid ribs and a flexible skin [7]. Airflow through the rotor can be blocked at the root and/or the tip. In full-scale experiments, it was found that plugging the root and leaving the tip open minimized these power penalties.

When negative pre-cone was used to reduce tip deflections, additional skids were required at the blade tips to prevent damage during rest and spin-up/spin-down. If the skids are of significant size, they might also double as winglets, which might offer additional reductions in induced power. Winglets have demonstrated some limited utility in traditional helicopters, with improvements in induced power countering added profile and interference drag. Winglet design requires a combination of advanced design tools and experiments to be successful in mitigating induced drag. Several skid designs were tested, and showed that none of the designs performed well as winglets, and that a slight degradation of performance was unavoidable.

## ROTOR STRUCTURAL DESIGN

The design of *Gamera*'s rotor blades faced a number of constraints and challenges. Due to the large size of the blades and the need for eight of them in the quad rotor configuration, the blades represent a significant portion of the total structural weight. In addition to the common design challenge of maintaining high stiffness while minimizing weight, the blades are the only components which must be

aerodynamically efficient. The severe thickness restriction imposed by the airfoil geometry limits the structural efficiency of the blade spar, particularly for bending loads. The smaller the bending deflections, the more significant the ground effect benefits will be. Furthermore, the centrifugal stiffening present in normal rotor blades is greatly diminished in *Gamera* due to very low rotational speeds and low blade mass. Larger blade tip deflections increase the overall height of the airframe and as a result, the weight. As a result of all of these factors, the structural design of the blades represented one of the key challenges to the success of *Gamera*.

**Blade Design**

Established human powered aircraft and model airplane construction techniques were used wherever possible, but the severe design constraints of *Gamera* motivated the development of several novel approaches. These will be discussed, beginning with the ultra-efficient spar design, followed by the monolithic foam leading edge, and finally the trailing edge structure.

Traditional composite beam designs such as circular and rectangular tubes and I-beams were initially considered for the blade spar, but were all found to be excessively heavy. Due to their continuous section geometries, they all have large surface areas which require large amounts of composite material to fabricate. Traditionally, thickness around these components is varied so that areas with highest stress are thick while shear webs are made as thin as possible. However, this geometry leads to low compressive failure loads due to the poor local buckling resistance of these broad, thin webs. While the global buckling load may still theoretically be very high (due to large second moment of area) local buckling and crushing of such thin-walled members leads to earlier than expected failures.

The design philosophy that led to the development of the truss based members used in the spars and throughout the vehicle was that the non-linear impact of thickness on buckling could be used to the designer's advantage if the structural material were brought together into discrete members instead of being dispersed widely around the perimeter of the beam. Locally increasing the thickness would give a highly nonlinear increase in compressive strength. Furthermore, this grouping of material could be accomplished in a manner creating highly optimized substructures. For example, in the spar design developed here, the chord members were made from unidirectional carbon fiber composites arranged spanwise into tubes. This provides optimized stiffness and strength for the global bending loads, and significantly increased local buckling strength. Similarly, the shear web of the beam is constructed from unidirectional carbon fiber epoxy composites arranged into bundles with a ±45° orientation, which is optimal for carrying shear loads. This orientation is also ideal for carrying torsional loads induced by the aerodynamic moments. Use of a triangular spar cross section provides maximum stability. The triangular cross section, shown in Figure 12 is aligned such that all of the carbon fibers which take the global compression loading is grouped into a single tube (as opposed to the tension material which is split in two). Once again, this is done to take advantage of the nonlinearities of buckling resistance. Figure 12 shows an isometric view of the completed truss spar.

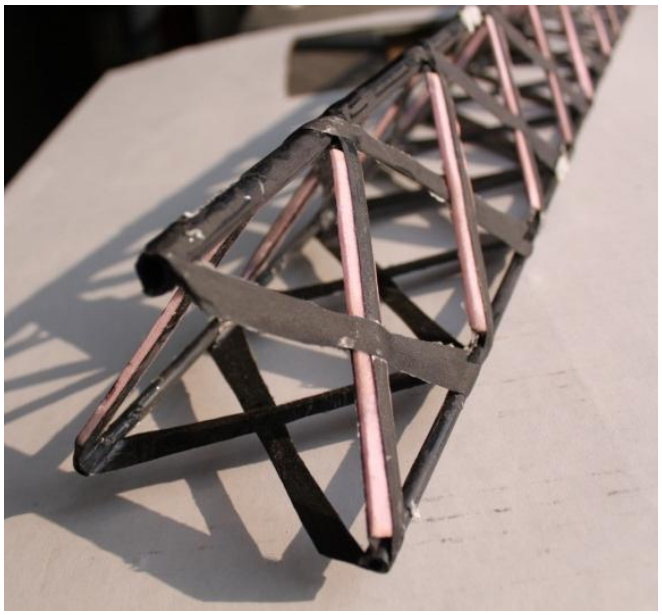

**Figure 12. Rotor blade truss spar**

The use of truss based structures lead to significant weight reductions in all of the major structural components. The primary problem with truss structures is the large number of components required for traditional built-up truss structures. The need to manufacture and then assemble all of these parts typically leads to long construction times and large man-hour requirements. A novel manufacturing process was developed for this truss spar and used throughout the vehicle which allows for large scale truss structures with hundreds of "members" to be built in only a few hours by use of a continuous winding process. The continuous composite trusses have no discrete joints or individual members in turn reducing labor, stress concentrations and weight while eliminating the need for fasteners or secondary bonding. Buckling prone truss members were built into sandwich structures with the addition of extruded polystyrene foam reinforcing strips during construction.

The rest of the blade structure was built up around the truss spar. The leading edge was manufactured from extruded polystyrene foam due to the excellent specific bending stiffness of this material. While thin Mylar film could have provided a lighter surface, the tight curvature and high pressure loading of the leading edge would have lead to significant geometric aberrations during tensioning of the Mylar and large deflections under aerodynamic loading. The leading edge was hot-wire cut from large blocks of foam, creating a single monolithic shell structure. This approach minimized the number of joints, reduced construction time and weight due to adhesives, and increased fidelity of the airfoil section. Another important feature of the leading edge

design can be seen in Figure 13 where the mechanical locking features in the leading edge are noted. Protrusions of the leading edge lock onto the spar geometry, such that the aerodynamic loading on the leading edge can be mechanically diffused into the spar. This reduces the reliance on adhesives and provides a precise positioning reference during assembly. The leading edge foam is also reinforced with lightweight foam ribs spaced along the span.

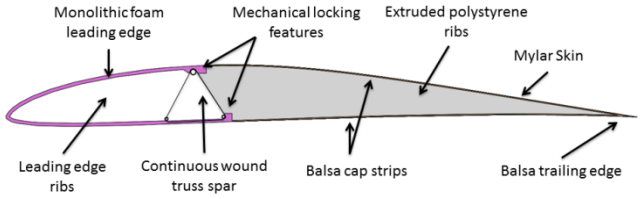


**Figure 13. Rotor blade structural design**

The trailing edge of the rotors is built up from lightweight foam ribs, a tapered balsa trailing edge, and a thin Mylar skin. The ribs are reinforced with balsa cap strips to increase bending stiffness and provide a smooth surface for Mylar bonding. The balsa trailing edge strips are carefully laid into the trailing edge ribs for efficient load transfer. The balsa strips are critical for resisting the chordwise tension in the Mylar skin and for restraining the ribs in the spanwise direction under centrifugal loading. The skin is made from the lightest Mylar film commercially available. This film is provided with a heat activated adhesive on one side for bonding to the structure. Heating the entire film after bonding shrinks the Mylar, removing wrinkles and any slack.

When a vertically upward load is applied to the structure, the top tube is under compression, and the bottom tubes are under tension. The terms "compression tube" and "tension tubes" refer to the nature of the stresses in the carbon tubes, under design loading (vertically upward).

### Rotor Structural Validation

While rotor blades are commonly modeled as long, slender Euler-Bernoulli beams, the current structure is more truss-like in construction, rather than beam-like. To verify whether Euler-Bernoulli theory could be used to model the spar, the spar components were individually modeled in ANSYS, using a connected set of unit cells. Each cell contains a compression tube, 2 tension tubes, and an X-shaped shear web connecting each side

Boundary conditions were enforced to satisfy displacement and slope continuity at the intersection of successive unit cells, and a vertical load was applied at the tip. A cantilever condition was enforced at the root of the structure. The analysis was repeated for various beam lengths, and the vertical tip displacement was compared to predictions from Euler-Bernoulli theory. It was found that agreement between ANSYS and theory improved as the length of the beam increased. The results are shown in the Table 1.

**Table 1. Convergence between Euler-Bernoulli and ANSYS modeling for long beam lengths.**

| Unit Cells | Tip Displacement (m) | EI (ANSYS) (Nm2) | % Deviation from E-B |
|---|---|---|---|
| 5 | 0.001 | 12758 | 35.46 |
| 10 | 0.01 | 17918 | 9.35 |
| 15 | 0.03 | 18079 | 8.54 |
| 20 | 0.06 | 18893 | 4.42 |
| 25 | 0.12 | 19276 | 2.48 |
| 50 | 0.93 | 19880 | 0.58 |

Bending tests on 3.3 ft (1 m) sub-scale spars were used to validate the ANSYS results and construction techniques before moving to full scale production. Mounted upside down, so that the compression tube was below the tension tubes, a standard set of weights were applied at the tip. The tip displacement was measured using a height gage and root slope measured with an inclinometer to eliminate inaccuracies caused by imperfect cantilever condition. Figure 14 shows the comparison of experiment and predictions from ANSYS on the sub-scale beam.

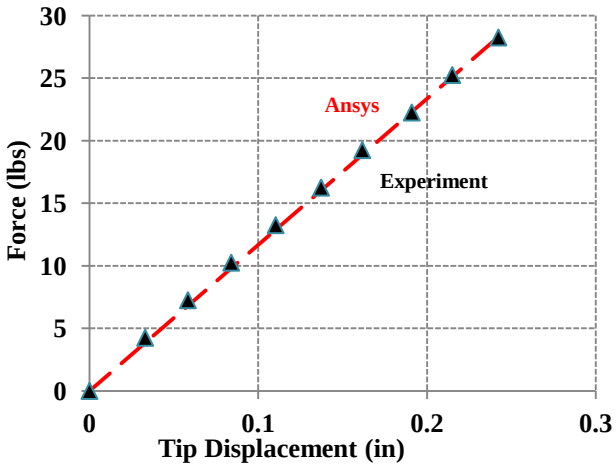


**Figure 14. Sub-scale spar tests correlated well with ANSYS Predictions**

Full scale validation used a ratcheting mechanism with a system of pulleys and an in-line load cell to apply and measure vertically upward loads at the blade tip. Because of the large tip deflections (up to 3 ft or 1 m) the pulleys were continuously shifted to produce purely vertical loading. At the blade tip a carbon tube (referred to as a cross-tube) was attached in the chord-wise direction. The chord-wise offset of the loading point on the cross-tube served to produce a pitching moment and bending load simultaneously. By varying the loading point on the cross-tube, the shear center of the spar (and later, the constructed blade) was found to lie close to the centroid of the spar. Maximum tip loads were calculated by setting tip deflection equivalent to that expected during flight.

In full-scale testing it was more accurate to measure the deflection at the mid-point and at the tip of the spar than of the root slope directly. The two-point deflection, combined with zero displacement at the root, was sufficient to back-calculate the stiffness of uniform beams from the load-deflection curve.

Initial tests of fully built rotor blades under vertical tip loads resulted in structural failures at load levels below the design limit. The failure was traced to joint failure where two sections of compression tubes were joined together using aluminum rod inserts. Adding carbon sleeves around these joints all along the blade, in conjunction with reinforcements near the root, sufficiently reinforced the weak points, adding 1lb to the entire vehicle weight.

The bending stiffness values of fully assembled blades varied between 3380000-366000 lb-in$^2$ (9700-10500 Nm$^2$). The Euler-Bernoulli theoretical prediction for the spar was 3310000 lb-in$^2$ (9500 Nm$^2$). This indicated that the leading-edge foam provides up to 10% bending stiffness if all the foam pieces are properly bonded together with epoxy. Any break in the continuity of the foam leads to partial loss of stiffness from the foam, and the scatter in blade stiffness is attributed to variations in the construction process, along with incremental stiffness provided by the leading-edge.

Restraining tip deflections to keep the working sections of the blade closer to the ground was investigated using cable tie-downs. Cables of different material (steel and two types of Kevlar) were used to restrain the blades. One end of the cable was attached to the tip of the blade, and the other end to a fixed point directly below the blade root. A beam FEM analysis was modified to incorporate the effect of tie-downs and solved iteratively to obtain deflection under tip loads. Analytically with tie-downs, the blades showed a noticeable increase in stiffness. Experimental results did not agree with the analysis, instead indicating that the overall deflections were reduced by a static offset without predicted increases in stiffness. The sensitivity of tie-down effectiveness to root slope, could not justify the extra weight of the cable and related attachments, 4.4 lb (2.0 kg) for 8 blades. Further the additional profile power of the cables and attachments rendered the implementation of tie-downs impractical.

## AIRFRAME

The choice of the airframe structure, its analysis, optimization and final design were driven by *Gamera*'s quad rotor configuration. Initial sizing analysis provided the required rotor radius of 21.3 ft (6.5 m). It was predicted that each truss arm would need to support 60 lbs (27 kg) tip load, when appropriate safety margins were accounted for. The challenge of the lightweight design was then to meet these loads without allowing structural deflections that jeopardize the efficiency of the rotors or endanger the aircraft.

To avoid airframe strikes, the deflection of the lifting rotor blades had to be taken into account during the design of the airframe. Rotor design suggested an expected mean tip deflection of 2.9 ft (0.9 m). This was complicated further by the observed lift imbalances that tilt the tip-path-plane motion making one blade more likely to strike. With appropriate safety margins, it was decided to account for 3.3 ft (1 m) of deflection at the tip of the rotor.

The pilot mass accounted for half of the total weight of the flying structure and had a large influence on the position of the center of gravity of the aircraft. The selected configuration already assumed that the pilot is centered between the rotors but in addition to this the design of the airframe was also took into account the vertical position of the pilot. Initial design sketches had the pilot suspended 5.2 ft (1.6 m) above the ground. Easy access to the cockpit and transmission for the pilot and repairs made this height unrealistic. Therefore the airframe was kinked at the rotor tips to have a flat cockpit section and limit pilot height.

The shape and size of the airframe required that it could not be built as a single continuous structure while still being transportable between the workshops and flight tests. This required that the structure include some provision for disassembly and reassembly into manageably sized segments.

### Airframe Design Method

The simplest and most efficient configuration of this airframe is four arms radiating from the central cockpit to the hub of each rotor where the vertical rotor loads are carried. A truss offers a light weight solution to this structural problem.

The primary design constraints already mentioned was the total length, which had to accommodate 21 ft (6.5 m) long blades and allow for clearance between the four rotors. This produced a design length of 31 ft (9.5 m) length. Unlike the rotor spar, the nodes are sparse and bucking lengths are long. Prefabricated tubes of appropriate size to resist this bucking were larger than required driving up weight. For this reason the truss was designed with two members in compression and one in tension to split bucking loads and allow more careful tailoring of the spar weight. The truss was analyzed by finding the total deflection at the tip while ensuring that the compressive loads did not exceed the material limits or the buckling resistance of the individual truss members.

Figure 15 shows the modeling of the truss. The arm was assumed to be pinned at the center of the airframe (cockpit) and free at the tip (rotor). The truss for *Gamera* was described by the configuration, the number of nodes distributed along the lower main member of the truss, the node positions and the truss element properties. The configuration included the continuous global dimensions of the truss such as the height, width and slope of the truss. This analysis made the assumption that the main upper and lower truss members are aligned with a constant slope which simplified construction and limited the number of variables required to describe the truss. The configuration enforced the node positions as continuous valued lengths along either of the main upper or lower truss members. In general, increasing the number of nodes increased stiffness, but this

also increased the truss weight. The final degrees of freedom were the truss element properties including the stiffness, area, area inertia and density of the truss members. For practical reasons, these parameters generally were limited to parameters of commercially available pultruded tubes.

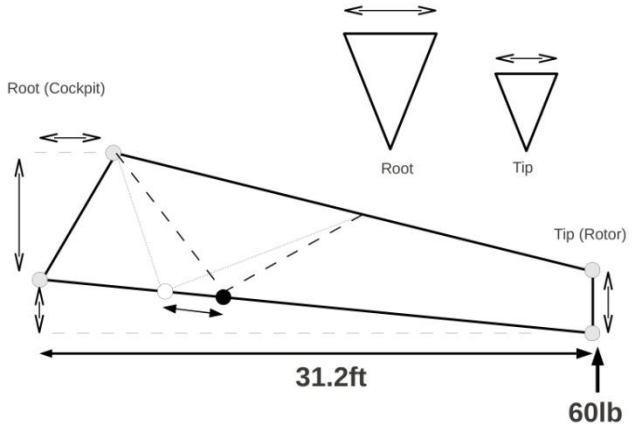


**Figure 15. Truss configuration schematic**

The truss arms were analyzed using a simple space truss code. A shortcoming of this tool was that the truss members were assumed to carry axial loads only and no moments were transferred across joints. While this assumption is valid for standard trusses, it can break down for a light weight and flexible structure. Experimental comparison to the truss analysis showed acceptable correlation and was bounded within the error associated with construction techniques.

Designing a buckling resistant truss within these constraints is a straightforward task with the challenge being to minimize weight. The large number of degrees of freedom and their continuous values make finding a minimum weight more challenging. Therefore a genetic optimization routine was used to select the truss configuration. This is detailed in the following section.

The advantages of a genetic algorithm are that it is relatively simple to implement and adapt to various problem configurations without requiring knowledge of the functional dependencies of the variables involved. It is well suited to discrete data and can reach a good solution faster than gradient based methods requiring special treatment for discrete data. The disadvantage is that the algorithm does not take advantage of the gradients in the vicinity of a candidate solution. For this reason a gradient based method will generally find a better minimum near the local minimum found by the genetic algorithm. This compromise was made in the truss design of *Gamera*.

As a generalization a genetic algorithm proceeds as follows. An initial population of candidate solutions, in this case trusses, are initialized using a random process of variable selection. This population is called a generation and each member a chromosome. Each chromosome is evaluated using an objective function and ranked according to their score, such as minimum weight or tip deflection. Then a process emulating natural selection creates the next generation of chromosomes. The next generation includes clones of top performers, children of two random fitness weighted parent, mutant children of one parent and entirely new random chromosomes. This process continues until some minimum threshold is achieved or, in this case, for a set number of generations based on history of weight reduction.

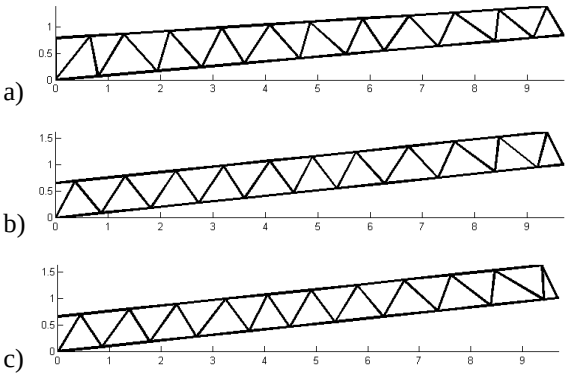


**Figure 16. Truss Evolution after a single generation (a), ten generations (b), and finally at one thousand generations (c)**

The most significant challenge in applying a genetic algorithm to the optimization of this truss was in describing the truss as a set of variables, a chromosome, suitable to use by the genetic algorithm. A random vector of variables describing the configurations may violate requirements that the truss be statically determinant. To overcome this, some bias in the configuration topology was introduced to avoid invalid trusses. The combination of discrete and continuous

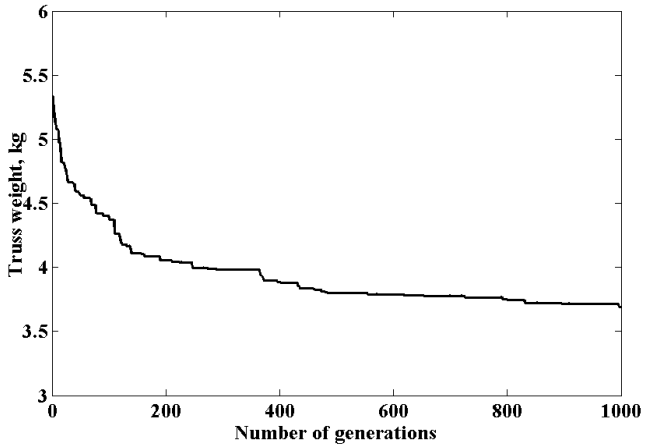


**Figure 17. Time history of a single run of the truss optimization code.**

variables required that some structure with appropriate encoding/decoding be included in the generation of the population in addition to setting appropriate bounds on the design variables to fit within both the physical and practical design constraints already mentioned. Once this was achieved, the truss configuration, node position and sectional properties were described by a single chromosome, or vector of variables, suitable for use by the genetic algorithm.

Figure 16 shows an example of the trusses evolution over successive generations. The population size of each generation is a modest ten for these results. In general identical runs of the optimization give different time histories of the truss configurations even for the final optimized truss. However the final weights achieved are generally quite close. Figure 17 shows the history of the weight of the highest ranked truss at each generation for these populations. A substantial 4.5 lb (2 kg) reduction in weight has been achieved over the 1000 generations. It is also evident that further reductions can be achieved and that the optimization was stopped prematurely.

The main control variable that most strongly governed weight during early truss design was the number of nodes distributed along the lower main member of the truss. In general, increasing the number of nodes increased stiffness and resistance to buckling at an increase in the total weight. Optimizing for minimum weight therefore generated an impractically low number of notes. The results of initial truss testing showed premature onset of buckling caused both by the self weight of the truss members which became significant over long unsupported lengths, and challenges in perfectly aligning tubes at joints between nodes. This was ultimately resolved by limiting element lengths to 4 ft (1.2 m) carbon tube sections available off-the-shelf which further constrained the minimum number of nodes.

Off-the-shelf pultruded carbon fiber/epoxy tubes, carbon fiber tow and tapes were used almost exclusively for the truss design due to the superlative structural efficiency of unidirectional carbon fiber composites. Carbon fiber tubes were sampled from various providers and tested to determine their stiffness and weight per unit length to be used during the design optimization. The joints at the truss nodes were constructed by inserting layers of unidirectional carbon tape acting as gussets between intersecting tubes and secured with carbon fiber tow lashings.

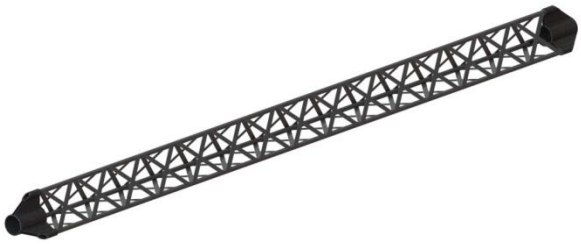

**Figure 18. Baby truss design**

A final significant development in the truss design came in the material options. The restriction placed on the design of using only commercially available carbon fiber tubes required very large tubes at the truss root compression members to provide enough area moment to resist buckling. These came at a significant weight penalty. To replace these heavy elements, scaled down versions of the blade spar were used, offering increased buckling resistance while reducing total weight. These "baby trusses", pictured in Figure 18 were subsequently adapted to replace all the center section compression members.

Ultimately the optimization was run several times and found to regularly converge on a consistent weight after 1000 generations with a population of 100. The nature of these optimizations meant that the solutions were not unique, so outputs of common weights were combined to generate the result shown in Figure 19.

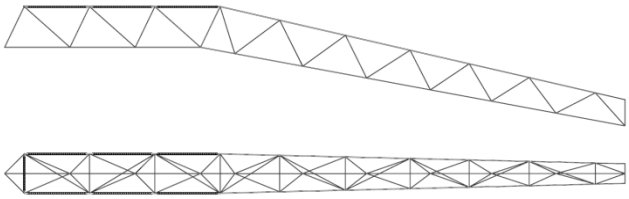

**Figure 19. Final truss design, note the use of baby trusses on the top of the 3 furthest left cells.**

**Testing and Evaluation**

Initially, a one-third scale version of the truss was constructed in order to validate the analysis, as well as develop and optimize construction techniques. The results showed that the truss carried the design load without buckling failures but the tip deflection was higher than predicted. These differences were small and were attributed to construction limitations and simplifications in the truss analysis. However these margins were found acceptable.

**Figure 20. Dynamic test of preliminary rotor, truss arm and transmission on the Quarter Rig**

Subsequently a final design, similar to that shown in Figure 16, was optimized and built to identify any concerns at full scale. The designed weight was 7 lb (3.2 kg) which was closely matched by the built truss weight of 8 lb (3.6 kg) (including the addition of small pulleys for transmission line and shaft mounts). This truss was first tested under design load in a static test, and then in a dynamic test using the rotor blades that were actually intended for use in the final vehicle. These tests were carried out using a custom test rig shown in Figure 20

In static tests the root truss members under compression buckled and were subsequently reinforced by the addition of nodes to shorten the effective lengths. Dynamic tests revealed a new failure mode resulting from rotor imbalance. Rotor imbalance introduced cyclic bending moments in the fixed frame, inducing a periodic torsional moment on the truss. This applied an off-design loading on the truss and created buckling in the diagonal members of the truss. To account for this in subsequent designs, a rotor imbalance was included in the loading applied during the truss evaluation. This additional modeling proved sufficient for the final truss design.

## TRANSMISSION

Driven by an inherently limited powerplant, the system consisted of three major regions. Within the cockpit, mechanical power had to be extracted from the pilot. At each end of the structure, the power had to be delivered to the rotors. In between, the power had to be split into four even streams and transmitted up to the main structure before splitting down each of the kinked truss sections to the rotors. Like all aspects of this design, it was essential to meet these goals while minimizing weight. The first step in the design process was deciding what method would be used to link the cockpit to the rotors, after which the rotor-side and pilot-side transmission assemblies were independently designed.

### Transmission Method

Options considered for the transmission included chain, belt, shaft, and string drive systems. Chain, belt, and shaft drives offer the benefit of continuous operation. The major disadvantages of the former two systems were mechanical complexity and weight. Both systems would require at least four sprockets or pulleys at the center of the cockpit linked to the feet of the pilot to provide power. Further difficulty would be caused by the need to reverse direction on two of the four rotors, requiring extra gears or belt crossing. From the central mechanism the chains or belts would have to reach several meters to the rotors and back, adding significant weight. Belts were favored for being lighter than chains, however they also had their own problems, including the possibility of slippage losing power and putting the rotors out of phase.

Weighing these concerns, it was decided to use a string driven system. The pilot side pulley used here is illustrated in Figure 21. Using string allowed a simpler design with no need to return a belt to the cockpit and no extra reversing mechanism, the cord was simply attached to the opposite side of the rotor pulley. Furthermore, the pulleys required to direct the string out to the rotors could be much simpler and lighter than those required for a timing belt. With low rotor RPM and short flight durations, string lengths of only 100 ft (30 m) are required. After considering several options it was decided that the high strength and low friction of Spectra fiber braided line made it the best choice for use in the transmission.

### Rotor Side Transmission

The rotor side pulley was made of an expanded polystyrene foam core with four spokes reinforced with carbon composite rods to carry bending loads and carbon fiber tow at ±45° to handle shear. Woven carbon fiber tape was also used to form a rigid composite rim on the pulley and molded to provide a slightly concave channel in which the string would be wound before each flight. At the center of the pulley hub, a square pocket was included to provide an interface for transferring torque into the rotor shaft. The shaft itself was a custom tube manufactured from biaxial and unidirectional carbon fibers.

**Figure 21. Cockpit featuring hand and foot cranks, truss based construction techniques, and highlighting the nature of the pilot side spooling pulley**

The square adapter at the end of the rotor shaft was molded out of carbon fiber composite and syntactic foam and is shown in Figure 22. This piece was bonded to the carbon shaft. Another square adapter was affixed to the far end of the shaft providing flat surfaces on which to attach the rotor hub. This second end adapter also provided an attachment point for the landing gear on which the helicopter rested between flights.

The blade hub was designed with the aid of testing on the previously mentioned BBR. Due to the low levels of centrifugal stiffening the blade flap and lag motions were constrained solely by the rigid hub. The unique cross section of the spar provided three discrete points of contact for each blade: one high point in compression and two low points in tension. The hub was designed to align the triangle of points on each blade with that opposite, thereby transmitting only

force and torque to the rotor shaft. Reducing these loads allowed weight savings in both the hub and the shaft.

The passive stability of the quad rotor design led to the decision to avoid the complexities of active control and instead utilize a fixed pitch hub. Fine adjustment of the pitch of each blade could be achieved between flights by using a pair of set screws to lock the three points of the spar at the desired angle. The entire rotor-shaft-blades assembly is shown in Figure 23.

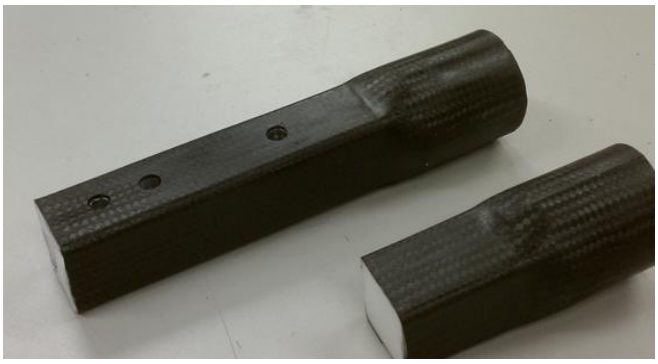

**Figure 22. Adapters used to transfer torque from the pulley to the shaft (below) and from the shaft to the blades (above)**

**Figure 23. Rotor side pulley, shaft, hub and landing gear**

**Cockpit**

Within the cockpit, the pilot delivered power by using both foot pedals and hand cranks. The pedal power was delivered using a Zipp VumaQuad carbon fiber crankset. The hand cranks were fabricated in house with a carbon fiber tube serving as the spindle running on bicycle bearings. Hand cranks were made from a balsa core wrapped in carbon fiber fabric with custom grips molded to the shape of the pilot's hands. The hand cranks and pedals were connected via a sync chain using two sprockets. These sprockets were initially made from a carbon fiber and balsa wood sandwich to allow light weight at a large diameter, lowering the force and thereby permitting a light, all plastic chain to be used. During flight testing, however, wear of the sprocket teeth and plastic chain were noticed, forcing a switch to aluminum sprockets of a smaller diameter and a heavier steel-plastic hybrid chain.

Flight testing also revealed a phenomenon that had not been accounted for in bench top testing, the inversion of the tension side of the chain. Ideally, the pilot would always be driving the feet with the hands. However, when operating at full speed, the pilot would sometimes lead with the feet, causing the tension side of the chain to reverse. As the original chain tensioner was only on the ideal return side, this caused the chain to occasionally jump off the sprockets at full power. A new chain tensioner on both sides of the chain and dynamically tensioned by springs was used to alleviate this problem.

The initial design of the cockpit featured a pulley with a basswood core connected to the bolt circle pattern of the crankset. Basswood was chosen due to its light weight and relative insensitivity to grain direction. This proved to be inadequate when operated at full power as the tension of the strings caused the core to crush, thereby breaking the flanges affixed to the end and causing the string to skip off of the pulley. An aluminum shell was machined to fit around a basswood core, a design which ultimately proved successful.

The cockpit used in the first round of flight testing consisted of single carbon fiber tubes connecting the seat, hand cranks, and foot cranks to the structure at three nodes. This was further secured by Kevlar guy-wires to provide lateral rigidity. Though this design was adequate under static loading it was demonstrated to be insufficiently rigid at speed; power was lost to the elastic deformations of the cockpit as it swayed back and forth. The lack of rigidity was especially problematic at the feet, where the pulley was mounted laterally next to the single tube so the tension from the strings tended to rotate the entire crankset. This moment combined with that occurring from the pilot's pedaling to cause an angular misalignment between the sync sprockets at the hand and feet, thus causing the chain to walk off the sprocket under load. After reinforcing the cockpit *Gamera* was still able to fly, but changing the design of the cockpit to feature stiff, 2D planar trusses with a center mounted pulley (Figure 21) was critical to allowing the greater success achieved in the second round of flight testing.

## PILOT

In describing the human's role in *Gamera*, the word "pilot" is used loosely. Focus required by the physical demand on the pilot coupled with the fixed pitch rotor hubs mean the pilot lacks any attitude or heading control, and serves primarily as the powerplant. As such the design goals relating to the pilot are to extract high levels of power as efficiently as possible while maintaining acceptable safety levels.

A distinguishing feature of *Gamera* is the use of hand cranks in addition to the more conventional foot cranks. This design decision originated in the Sikorsky Prize flight requirements. Flight duration of 60 seconds puts the human in a very different regime, in a physiological sense, than other human-powered vehicles. Exercise physiologists have estimated that for short-duration exercises, between 20-60 seconds, energy production is fueled almost entirely by anaerobic glycolysis [8]. This process relies on the glycogen stores within the active muscles. The implication is that engaging more muscle mass should release more stored energy (glycogen). This is in contrast to prolonged-duration activities (several minutes to hours) where the energy production is primarily aerobic and therefore limited by oxygen supplied by the pulmonary system rather than muscle mass.

There are relatively few controlled experiments found in the literature comparing short-duration power output of exercises with and without the additions of the upper body. Ursinus's experiments from 1936 are commonly cited in human-power publications. He performed experiments on one subject involving several apparatus, but notably compared leg cranking with leg and hand-cranking [9 and 10]. Wilkie re-drew Ursinus's data in 1960, showing that the addition of hand-cranking yielded about 30% more power output than cycling alone for a 60-second effort, with increasing gains at shorter durations [11]. Evans [12] compared the results from Ursinus as well as experiments by Bergh [13], and concluded that for human-powered aircraft "useful improvements in power-to-weight ratio may be obtained by the addition of arm work," estimating 50% more power for durations of 90-seconds. Harrison conducted experiments comparing rowing (legs and arms) and cycling (legs only), also concluding that for maximum power output of activities under 5 minutes the participant should make use of as large a muscle mass as possible [14].

Despite this evidence pointing towards improvements in power with the addition of hand cranks, it gave the team pause that no other successful human-powered aircraft has employed hand cranks. The reasons for this absence on fixed-wing aircraft is fairly clear. For one, human-powered fixed-wing aircraft durations were measured from minutes (7 min 27 seconds for the Kremer Prize-winning flight of the *Gossamer Condor*) to hours (*Gossamer Albatross*, MIT *Daedalus*). This is well within the aerobic regime where the addition of muscle mass has limited benefits. More importantly, these pilots were pilots in the true sense; they required their hands free to operate control levers in the cockpit. The previous two successful human-powered helicopters, the *Da-Vinci III* and the *Yuri I*, both utilized leg cranks only. There were no publications found to indicate whether those designers had considered adding hand cranks.

### Pilot Test Rig

The potentially large power output gains of adding hand cranks motivated the team to integrate a pilot test rig into the Quarter Rig test stand (shown in Figure 24) to evaluate the concept. Ultimately the pilot test rig was used to:

1. Quantify the benefits of adding hand cranks
2. Measure any differences between recumbent and upright cycling
3. Determine optimum pedaling RPM
4. Provide a training rig for the final pilots

**Figure 24. Test Pilot Judy Wexler Training on the pilot test rig**

Team members were initially used for power testing on the rig since pilots had not yet been recruited. The results from the testing verified that the addition of the hand cranking increased power output from 10-20% depending on the pilot. These tests also showed that a recumbent position did not incur noticeable losses when compared to an upright position, a result that agreed with published studies. A representative result from a test run is shown in Figure 25. The pedaling frequency was varied and it was determined the optimal was 120 RPM for durations of up to 20 seconds. This finding agreed well with studies by Martin [15].

The team made use of a commercial stationary recumbent cycling machine in the University of Maryland Epply Recreation Center for pilot comparisons. The machine had a digital output display for pedaling RPM and power output in Watts. The accuracy of the power measurements from the recumbent machine was unspecified, but A-to-B comparisons between pilots were sufficient to down-select a final set of pilots. Judy Wexler, Kyle Glusenkamp and Colin Gore were selected and trained to fly (power) *Gamera*.

In flight the pilot of *Gamera* would be required to output a constant power level to maintain a hover at a specified height. Therefore, testing was performed at a constant resistance until an RPM of 120 could no longer be maintained. That test to exhaustion would produce one point

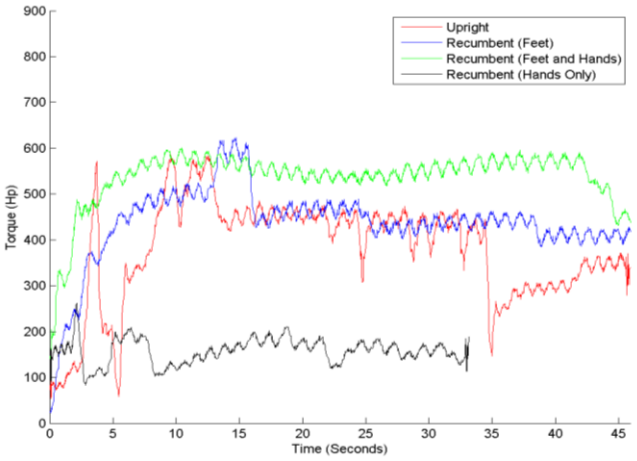


**Figure 25. Typical data from one pilot taken on the pilot test rig and used for configuration decisions**

on a power versus duration plot. Such a plot from our final group of selected pilots is shown in Figure 26. Note the x-axis is duration at a constant power, not elapsed time. Since the pilot group had varying body weights, the metric of importance is specific power. Our down-selected pilots were in comparable ranges of specific power, with Judy Wexler showing a slight edge at shorter durations. She was also the lightest of the three, at 50 kg (110 lbs). At the time of pilot selection, the vehicle structure and rotor system design had been frozen and construction was well underway (due to programmatic constraints on schedule). With a structure designed to a pilot of 130 lb (59 kg) concerns surrounded the use of pilots weighing 135 lb (61 kg) each. Coupled with an edge in specific power, Judy was selected to be the primary pilot.

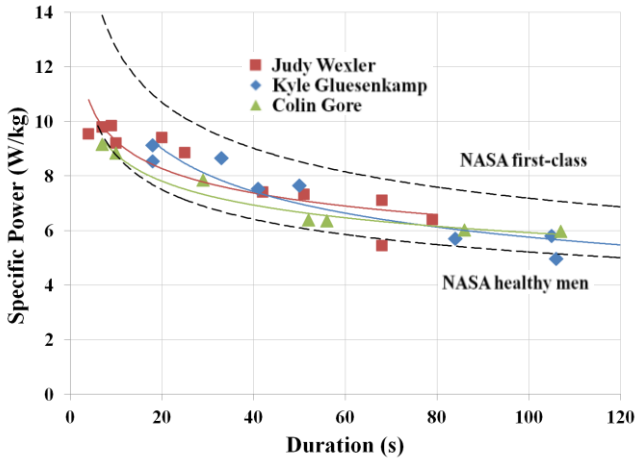


**Figure 26. Specific power vs. endurance for the 3 selected pilots compared with data compiled by NASA [16] for healthy men and first-class athletes.**

Average specific powers for the pilots tested (and between published NASA data for healthy and first-class men [16]) ranged from .0055 hp/lb (9 W/kg) for short duration flights and .0043 hp/lb (7 W/kg) for a 60 second flight as shown in Figure 26. From the pilot test rig experiments and the literature, a power output increase of 20% from the addition of hand cranks was assumed. Therefore, with Judy Wexler as pilot, maximum power available was estimated at 0.76 hp (565 W) for a 20-second flight, and 0.79 hp (590 W) for a 10-second flight.

## SYSTEM INTEGRATION AND FLIGHT TEST

First a full-scale, quarter-vehicle test was used to validate the initial design concept and approach. In 2011, *Gamera* was assembled on two separate occasions at large on-campus facilities, (basketball arenas) chosen to accommodate not only the geometric footprint of the vehicle, but its expected drift in hover. The first flight test was performed in the auxiliary gymnasium of the Comcast Center from May 5 to May 12, 2011. This test demonstrated that *Gamera* is capable of flight and helped identify key areas for design improvement. These changes were implemented and *Gamera* flew again in the Reckord Armory from July 5 to July 13, culminating in a world-record-setting flight.

### Quarter Rig Testing

A functional quarter of the vehicle (Quarter Rig) was built in the fall of 2009 to test a single rotor (with associated support structure), evaluate pilot power output and measure rotor performance. This rig consisted of a steel frame with upright and recumbent pilot positions, as well as optional hand cranks. The pilot output could be diverted to a dynamometer or a quarter arm of the airframe, supporting one rotor. The Quarter Rig is shown earlier in Figure 20 with truss and rotor attached, and in Figure 24 with a pilot in the recumbent position. The shaft was instrumented with strain gages for measuring torque and a Hall sensor for RPM. The entire apparatus is mounted on four load cells under the frame and one load cell under the rotor for thrust.

The Quarter Rig was used for system tests in the winter and spring of 2010. The dimensions of the rotor precluded several open and closed spaces available to the team. First, a limited number of outdoor tests were attempted at Hornbake Plaza on the University of Maryland campus. The plaza is a recessed bowl surrounded by buildings that limit the amount of wind and tests were performed during the calm of early morning. A gust of 1 m/s translated to an effective advance ratio of 0.1, causing a large hub moment in the rotor. These tests validated the design and interaction of the transmission systems, but high RPM and high thrust cases were unobtainable because of the extreme gust response. During tests in spring 2010, performed at the Cole Field House, operational RPM was reached and sustained, validating the rotor and airframe abilities to survive dynamic loading. Challenges existed in measuring total thrust after the rotor thrust exceeded its weight, and broke contact with the load cell. The significant mass of the steel pilot frame and problems in precisely controlling pilot RPM motivated development of the BBR.

### Vehicle Trim

For full vehicle flight test, the vehicle was assembled and carefully trimmed during a series of 80 preliminary

tests. The tests also allowed for integration and trouble shooting of transmission elements. Throughout these tests, it was critical to measure vehicle thrust and moments, rotor RPM and blade tip deflections. Thrust was measured by four load cells under the landing gear for each rotor and an optional fifth load cell under the cockpit, limiting exposure of the structure to high stress for long periods of time. Each load cell was measured through a National Instruments DAQ system. Coupled with measurements of load cell positions, both thrust and vehicle moments were calculated. Direct measurement of RPM was not feasible due to the additional weight and complexity associated with the instrumentation. Pilot RPM was therefore managed by playing a metronome and asking the pilot to match that cadence at the pedals, while rotor half-periods were measured by team members using stopwatches. Tip deflections were measured to qualitatively evaluate rotor tracking and limit the risk of collisions with the airframe.

Baseline pitch angles were measured for each blade pair during BBR tests and a characteristic thrust versus RPM curve was generated. Using these tables as a starting point, each rotor was individually trimmed, and then paired with the diagonally opposite rotor. Finally, all four rotors were spun and balanced simultaneously. Within each set of tests, the RPM was progressively raised and the pitch settings of the blades iteratively adjusted until the required rotor forces were obtained. The advantage of using this procedure was that each aerodynamic component could be modified independently. This allowed the transmission and airframe elements to be evaluated with increasing load levels.

The airframe was designed to allow for truss arm tip deflections of 0.3 ft (0.1 m) under actual thrusts. This allowable deflection becomes problematic when the pilot's weight is offloaded through the fifth load cell. During single rotor tests the rotor hub can deflect up to 0.7 ft (0.2 m), from the deflection of its support arm, in addition to that of the opposing arm. In paired rotor tests, this deflection caused the vehicle to trim to non-zero pitch and roll attitude through differential ground effect.

Another problematic aspect of opposing rotor tests was that both rotors spun in the same direction, leading to a buildup of vehicle yawing moment. This moment caused the vehicle to spin about the pilot at high thrusts. Vehicle pitch and roll were therefore much easier to balance during a 4 rotor test. Once all 4 rotors provided balanced thrusts at thrusts approaching hover requirements, *Gamera* was ready for free flight.

### Flight Tests

Flight tests required further adjustments to rotor pitch settings, which were performed iteratively based on observations of vehicle attitude and drift directions. Yaw was managed by adjusting the blade pitch angles on two diagonally opposite rotors, and no couplings with pitch and roll were evident. Pitch and roll imbalances induce slight attitude changes in the vehicle. This rotation caused opposing rotor hubs to move closer and farther from the ground, respectively, introducing differential ground effect. In the extreme case, the attitude change was sufficient to induce drift. In most testing, the forward rotor consistently required a higher pitch setting than the rear rotor, since longitudinal balance was sensitive to a slight forward bias of pilot location in the cockpit.

Vehicle thrust was adjusted using pilot RPM and could be increased by as much as 1.5% for a 1% increase in pilot RPM. As a consequence, increases in pilot RPM above the design setting elevated the vehicle, equalizing thrust but dramatically increasing power required. To avoid expending this additional power for no additional benefits, the pilot was instructed to manage her pedaling RPM and so maximize endurance.

After several partial lift-offs, there were 2 successful flights during the testing at the Comcast Center. The first was of short duration and video evidence was deemed inconclusive. The second flight was successful, and certified as 4.2 seconds by the FAI. Each rotor landing gear was monitored through a dedicated video camera, all four of which were synchronized to validate the successful flight.

Several design features were improved after the first successful flight test. Identifying which rotors were airborne during the flight was challenging due to the small displacements compared to vehicle dimensions. In the second round of testing, pressure sensitive LEDs were placed at the tip of each landing gear, set to illuminate when the rotor left the ground. Coupled with video monitoring, this method of determining a successful lift-off was highly effective. The cockpit was rebuilt to decrease deflections under load. Finally, significant amounts of negative precone were applied to limit absolute tip deflections during flight. This precone deflected the rotors so far against the ground that low friction skids were added to the tips of the blades and rested on smooth plastic strips to decrease friction induced startup torque.

Throughout the round of testing in the Armory, *Gamera*'s robust design was validated by a series of significant but easily reparable accidents. Lightweight composite components fatigued over the long series of trim tests and a transmission failure during one flight caused the airframe to collapse. Fortunately, modular design allowed complicated parts to be easily interchanged with spares, while rotor components were repaired overnight. The next day, five short flights culminated in a world record flight time of 11.4 seconds.

## CONCLUSIONS

*Gamera* is a successful HPH that has set world records for a female pilot, with a flight of 11.4 seconds. Several key technologies were developed to minimize power required and to maximize the power available. These included careful modeling of a flexible rotor in ground effect, evaluation of full scale rotors, light weight blade construction techniques, careful truss weight optimization, ultra-light transmission, and pilot training. With all these aspects working together

and added benefits of ground effect, it became possible for *Gamera* to execute sustained hover.

While likely capable of hovering up to 30 seconds, simulations and experiments agree that the current *Gamera* is not likely to meet the requirements for the Sikorsky Prize. Its development has provided experience into novel construction techniques and analytic tools that can be used to design a Sikorsky Prize capable vehicle. In itself, construction, testing and successful flight of *Gamera* is a proud achievement of the team and the Alfred Gessow Rotorcraft center.

## APPENDIX

| Dimensions | | |
|---|---|---|
| Truss Arm Length | 31.4 ft | (9.5 m) |
| Overall Height | 7.5 ft | (2.3 m) |
| Number of Rotors | 4 | |
| Number of Blades ($N_b$) | 2 | |
| Rotor Radius (R) | 21.3 ft | (6.5 m) |
| Chord (c) | 3.3 ft | (1 m) |
| Airfoil | Eppler387 | |
| Taper Ratio | None | |
| Linear Twist | None | |
| Solidity ($\sigma = N_b c/\pi R$) | 0.0979 | |
| Rotor Speed | 17-18 (RPM) | |
| Empty Weight | 107.2 lb | (48.7 kg) |
| 8x Rotor Blades | 58.3 lb | (26.5 kg) |
| 4x Rotor Shafts | 3.7 lb | (1.7 kg) |
| Airframe | 31.9 lb | (14.5 kg) |
| Cockpit | 9.5 lb | (4.3 kg) |
| Other | 3.7 lb | (1.7 kg) |
| Pilot Weight | 106.9 lb | (48.5 kg) |
| Gross Takeoff Weight | 214.1 lb | (97.2 kg) |

## ACKNOWLEDGEMENTS

The team would like to thank Dr. Inderjit Chopra and Dr. VT Nagaraj for their constant advice and support and Dr. Daryll Pines for his unwavering passion. This paper is dedicated to the *Gamera* team members, past and present, who helped make *Gamera* a reality.

## REFERENCES

1. Filippone, A., "On the Possibility of Human-Powered Vertical Flight," *Journal of the American Helicopter Society*, Vol. 52, (4), October 2007.
2. Leishman, J.G., *Principles of Helicopter Aerodynamics*, Cambridge University Press, 2006.
3. Gilad, M., "Evaluation of flexible rotor hover performance in extreme ground effect," MS thesis, University of Maryland, 2011.
4. Selig, M.S. and McGranahan, B.D., "Wind Tunnel Aerodynamics Tests of Six Airfoils for Use on Small Wind Turbines," NREL/SR-500-34515, October 2004.
5. Goto, H., Kato, D., Abe, K., Kawasima, T., Motohashi, T., and Naito, A., "Power Measurements of Yuri I," Nihon University, Japan, 1994.
6. Hawkins, T.J., "Aerodynamic and Power Considerations for Human Powered Helicopter in Vertical Flight," MS Thesis, Stanford University, 1996.
7. Dingeldeign, R. C., and Schaefer, R. F., "High-Speed Photographs of a YR4B Production Rotor Blade for Simulated Flight Conditions in the Langley Full-Scale Tunnel," NACA-MR-L5C12c, March 1945.
8. Marieb, E.N., and Hoehn, K., *Human Anatomy and Physiology 8th Edition*, Benjamin Cummings Publishing, 2009, pp. 298-300.
9. Ursinus, O., "Grundung des Muskelflug" – Institute Frankfurt a.M, etc. Flugsport, 1-28, 1936.
10. Ursinus, O., "Versuche mit Energie-speichern, etc." Flugsport, 33-40, 1937.
11. Wilkie, D.R., August 1960, "Man as an Aero Engine", Journal of the Royal Aeronautical Society, Volume 64 No. 596, pp. 477-481.
12. Evans, A., "The Human Power Plant", Royal Aeronautical Society Human Powered Aircraft Group Conference, 1989.
13. Bergh, U., Kanstrup I., and Ekblom B., "Maximal Oxygen Uptake During Exercise with Various Combinations of Arm and Leg Work," *Journal of Applied Physiology*, 41(2), 191-196, 1976.
14. Harrison, J.Y., "Maximizing Human Power Output by Suitable Selection of Motion Cycle and Load," *Human Factors*, 12(3), 315-329, 1970.
15. Martin, J.C., and Spirduso, W.W., "Determinants of Maximal Cycling Power: Crank Length, Pedaling Rate and Pedal Speed," Applied Physiology (2001): 413-18.
16. Parker, J.F., West, V.R., and Webb, P., "Bioastronautis Data Book Second Edition," NASA SP-3006, 1973, Chapter 18.